Current-Driven Vortex Oscillations in Metallic Nanocontacts

Q. Mistral,[1] M. van Kampen,[2] G. Hrkac,[3] Joo-Von Kim,[1,*] T. Devolder,[1] P. Crozat,[1] C. Chappert,[1] L. Lagae,[2] and T. Schrefl[3]

[1]*Institut d'Electronique Fondamentale, UMR CNRS 8622, Université Paris-Sud, 91405 Orsay cedex, France*
[2]*IMEC, Kapeldreef 75, B-3001 Leuven, Belgium*
[3]*Department of Engineering Materials, University of Sheffield, Sheffield S1 4DU, United Kingdom*

(Received 30 October 2007; published 23 June 2008)

We present experimental evidence of subgigahertz spin-transfer oscillations in metallic nanocontacts that are due to the translational motion of a magnetic vortex. The vortex is shown to execute large-amplitude orbital motion outside the contact region. Good agreement with analytical theory and micromagnetics simulations is found.

DOI: 10.1103/PhysRevLett.100.257201 PACS numbers: 75.75.+a, 72.25.Pn, 75.60.−d, 85.75.−d

Lateral confinement in magnetic nanostructures leads to the appearance of complex magnetic states. The magnetic vortex is one pertinent and well-studied example, which has gained renewed interest due to improved lithography and fabrication techniques. The dynamics of such topological objects is, in part, governed by the confining potential. For instance, magnetic vortices possess a translational mode by which the vortex core executes a spiralling motion about its equilibrium position [1,2]. Recent experimental studies have demonstrated resonance phenomena with such cores [3–7], and proposals have been made for magnetic resonators based on these objects.

Recent experiments have shown that magnetic vortices can be brought into a self-oscillatory state [8]. This is achieved with the spin-transfer effect, whereby a spin-polarized current transfers spin-angular momentum to the magnetic structure, giving rise to an additional torque exerted on the magnetization [9,10]. The spin transfer compensates the natural dissipation processes under certain conditions, leading to self-sustained oscillations. The self-oscillator here is driven by a constant electric current only, in contrast to a resonator in which oscillations are driven by a periodic external force. While current-driven oscillations related to spin waves in magnetic multilayers are well-studied [11–13], Ref. [8] provides the first conclusive evidence of self-sustained oscillations for a topological structure.

In the context of spin transfer, confinement can also arise from the distribution of applied current itself. One pertinent example is the metallic point contact in which the current is applied through a small metallic cross section in contact with a continuous magnetic film [13]. In the absence of any applied currents, a vortex can exist in a continuous film, but, aside from sample edges and point defects, there is no magnetic potential in which vortex oscillations can take place. In the presence of an applied current, however, the Oersted fields produce an attractive potential centered at the contact center. Earlier experimental studies have provided hints at the existence of vortex modes, but no quantitative explanations for the observed low-frequency excitations were given [14]. In this Letter, we show that the cylindrical nature of the Oersted fields, generated by the applied current, is favorable to the creation of a magnetic vortex and provides a potential in which the vortex oscillates. Moreover, we demonstrate that the subgigahertz frequencies of these vortex self-oscillations result from a vortex orbit that is actually *outside* the contact region.

The experimental system studied is a metallic point contact deposited on a metallic spin-valve stack. The multilayer is composed of Ta(3.5 nm)/Cu(40)/Ta(3.5)/$Ni_{80}Fe_{20}$(3)/IrMn(7)/$Co_{90}Fe_{10}$(3.5)/Cu(3)/$Ni_{80}Fe_{20}$(4)/Pt(3). The NiFe (4 nm) layer is the magnetic free layer, and the CoFe layer, which is exchange biased by the IrMn antiferromagnet, serves as a reference layer for the giant magnetoresistance and spin transfer. The layers are sputter grown in an ultrahigh vacuum system with a base pressure

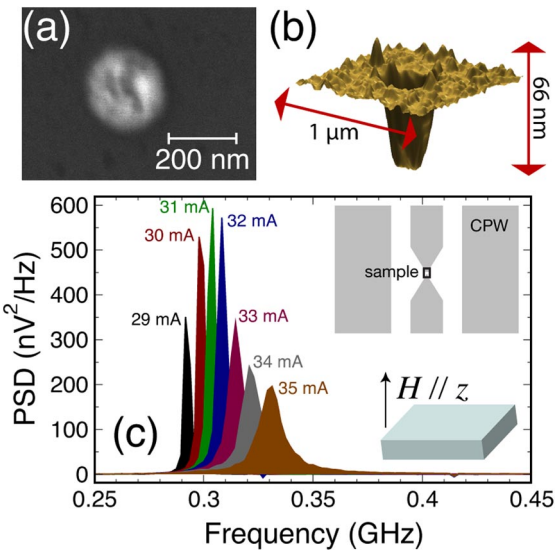

FIG. 1 (color online). (a) SEM and (b) AFM image of point contact. (c) Low-frequency PSD (power spectral density) measured at $\mu_0 H = 0.21$ T for several applied currents. Inset of (c): CPW and applied field geometry.

of 3×10^{-8} Torr. The sample mesa is rectangular and has dimensions of 27×17 μm. The contacts are made to the laterally extended stack which is incorporated in the central conductor of a coplanar waveguide (CPW) structure [see the inset in Fig. 1(c)]. After patterning by conventional lift-off lithography, the stack is passivated by a 50 nm SiO_2 layer deposited using rf sputtering. The point contacts are defined in a poly(methyl methacrylate) (PMMA) layer by electron-beam lithography and etched into the SiO_2 by a short dip in a buffered HF solution. The CPW structure is then deposited and patterned by lift-off lithography. Finally, the devices are annealed at 250 °C for 10 minutes to improve the exchange bias coupling between the IrMn and the $Co_{90}Fe_{10}$ layers.

The morphology of our point contacts has been characterized in detail by scanning electron microscopy (SEM), atomic force microscopy (AFM), ellipsometry, and optical microscopy measurements. The target diameter of the point contacts is nominally 100 nm; however, because of the isotropic wet etch, the diameter of the contacts is increased with respect to the 100 nm holes in the PMMA layer. Indeed, a significant variation in the diameter as a function of depth is found. In Figs. 1(a) and 1(b), we present an SEM and AFM measurement, respectively, of a typical point contact. While a diameter of 232 nm is extracted from SEM, AFM measurements show that the diameter can vary from 130 to 270 nm over a thickness of 40 nm. Based on the depth profile and our multilayer configuration, we estimate the contact diameter at the free layer to be approximately 200 nm.

For the magnetic properties, a uniaxial anisotropy field of $\mu_0 H_k = 1.4$ mT for the free layer is determined from hard-axis hysteresis loop measurements. From the easy-axis loops, we find the biased layer switching to be around -60 mT. A small bias of 6 mT in the free layer switching is also observed and is attributed to Néel coupling between the magnetic layers. The free layer saturation magnetization is found to be $\mu_0 M_s = 1.1$ T from alternating gradient field magnetometer measurements. For the electrical measurements, the applied current perpendicular through the spin-valve stack is generated by applying a dc voltage to a 200 Ω resistor in series with our sample. A 20 mΩ magnetoresistance is typical for our spin valves. Two bias tees allow dc and rf routing. One of the rf routes is amplified (+43 dB over the 100 MHz–26 GHz band) and connected to a spectrum analyzer. The other rf route is terminated by a 50 Ohm load while the dc route is shorted. The final power spectra are obtained after subtracting a reference curve taken with a zero current bias. The rf measurements are made for magnetic fields applied perpendicular to the film plane, which improves the magnetoresistance signal because the projection of the free layer oscillations onto the fixed layer is larger. Positive currents describe electrons flowing from the fixed to the free layer.

An example of the low-frequency power spectra that we have observed is presented in Fig. 1(c). The peaks shown represent the fundamental mode for several applied currents under a perpendicular field of $\mu_0 H = 210$ mT. Harmonics to fourth order are also observed, but these are several orders of magnitude smaller than the fundamental. The oscillations have quality factors up to 250, which corresponds to the narrowest linewidth of 1.2 MHz observed at a frequency of 299 MHz. These subgigahertz modes are suggestive of vortex motion rather than uniform precession [6]. Indeed, the Smit-Beljers equation [15] for uniform magnetization precession predicts a precession frequency of 1.08 GHz with our experimental parameters, which is clearly 4–5 times higher than what we observe. In contrast to earlier experiments in which nominally smaller diameter contacts were studied [13], the Oersted fields in our samples are significantly larger (at equivalent current densities) at the contact edges and therefore favor vortex formation. For example, a 30 mA current generates an Oersted field of 60 mT at the contact edge, which is a significant fraction of the perpendicular applied fields that we considered. We studied the power spectra over an applied current range of 0–40 mA. Similar oscillations are also observed for negative currents.

Three other key experimental observations support the hypothesis of vortex oscillations. First, the measured frequencies increase as a function of current for all applied fields considered ($\mu_0 H \leq 350$ mT). An example of this behavior is given in Fig. 2 in which the variation in the full power spectra is shown. The observed frequency blueshift is a feature of precession out of the film plane but is not expected for the fields used in experiment. Indeed, the

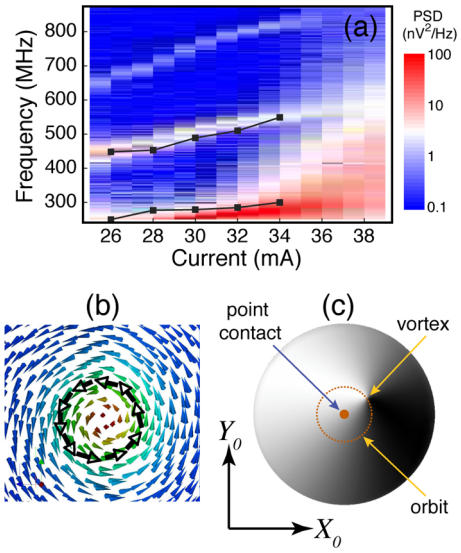

FIG. 2 (color online). (a) Color map of experimental PSD for $\mu_0 H = 350$ mT. Solid squares are results of micromagnetics simulations. (b) Top view of the vortex magnetization profile in the free layer obtained from simulation. (c) In-plane component of magnetization (black for $m_y = +1$ and white for $m_y = -1$) for the entire simulation area for $I = 30$ mA. Also shown are the contact and the vortex orbit (158 nm in radius).

spin-torque oscillator theory of Ref. [16], for uniform magnetization precession, predicts a frequency *redshift* for these applied perpendicular fields. Second, the precession mode is sensitive to small in-plane applied fields. The oscillations are observed to be stable for applied in-plane fields up to 15–20 mT in magnitude, and for larger fields the oscillations are completely suppressed. Furthermore, the narrowest peaks are obtained for in-plane fields that compensate the 6 mT bias field due to the Néel coupling, which is again consistent with the vortex picture. Third, the observed field and current hysteresis associated with the existence of oscillations is suggestive of vortex nucleation processes. For example, an oscillation threshold for increasing fields is observed, in the presence of an applied current in the 10–20 mA range, but these oscillations persist as the field is reduced below this threshold. Similar hysteresis is observed for the current variations.

To better understand the nature of the low-frequency oscillations, we performed full micromagnetic simulations of a trilayer CoFe(3.5 nm)/Cu(3)/NiFe(4) stack. The saturation magnetization of the free layer is taken to be the same as the experimental value $\mu_0 M_s = 1.1$ T, and a GMR ratio of 1% is used. We account for the inhomogeneous current distribution flowing through the free layer by computing the local current density from the local angle between the free and fixed layer magnetizations. The Oersted field is computed with the Biot-Savart law from this current distribution [17], and an asymmetric Slonczewski term for the spin transfer is used [18]. The simulation area is a circular film 1000 nm in diameter, with the 200 nm diameter point contact at the center. The system is discretized with a finite element method with a linear basis function and a discretization size of 4 nm, which is below the exchange length of 4.5 nm. An exchange bias field of 162 mT is applied to the reference CoFe layer to simulate pinning in the experimental stacks.

The simulations are performed as follows. First, we calculate the remanent state with an external field applied perpendicular to the film plane and in the absence of currents. From an initial uniform state in the film plane, we allow the magnetization to relax toward the applied field direction through time integration of the equations of motion. During this process, a vortex first forms under the point contact (situated at the center of the simulation grid) and is followed by the creation and annihilation of multiple vortices. After this transient phase, a single vortex state emerges as the system relaxes to its remanent state. Next, currents ranging from 26 to 36 mA are applied, with the remanent state serving as the initial state for this step of the calculation. We observe that the additional spin torque drives the vortex out of the contact area and towards a stable orbit around the contact.

These simulations reveal that the oscillations observed are related to the large-amplitude translational motion of a magnetic vortex. In contrast to the nanopillar geometry in which the vortex core precesses within the confining part of the Oersted field [8], the dynamics here correspond to an orbital motion *outside* the contact region. This behavior can be likened to planetary orbital motion under the influence of a gravitational field; the spin-transfer torque leads to a centripetal motion of the vortex core, which is counterbalanced by the attractive potential provided by the Oersted field. Good quantitative agreement between the simulation and experimental frequencies is achieved, as shown in Fig. 2. The stability of the vortex has also been investigated using simulations. For small in-plane fields (<10 mT), a small blueshift in the frequency is observed. This leads to an asymmetry in the field profile relative to the vortex structure and results in an elliptical motion of the vortex orbit. We have also verified in simulation that larger in-plane fields lead to a breakdown of the vortex structure.

A qualitative understanding of how the oscillation frequencies change with applied field and current can be achieved in terms of a rigid vortex model. Let $\Theta(\vec{r})$ and $\Phi(\vec{r})$ denote the magnetization orientation in spherical coordinates, with the spatial variations in $\vec{r}$ given in polar coordinates (ρ, φ) to exploit the symmetry of the point-contact and Oersted fields. We take the magnetization to be uniform across the film thickness. We derive an equation of motion for the vortex core by following Thiele's method [19]:

$$\vec{G} \times \frac{d\vec{X}_0}{dt} - \alpha \mathbf{D} \cdot \frac{d\vec{X}_0}{dt} + \sigma I(\vec{P}_\perp - \vec{P}_\parallel) = \frac{\gamma}{M_s} \frac{\partial W}{\partial \vec{X}_0}, \quad (1)$$

where $\vec{X}_0 = (X_0, Y_0)$ represents the vortex core position in the film plane, γ is the gyromagnetic ratio, α is the Gilbert damping constant, σ is a measure of spin-transfer efficiency, $\vec{G} = \int dV \sin\Theta(\nabla\Phi \times \nabla\Theta)$ is the gyrovector, $\mathbf{D} = \int dV(\nabla\Theta \bigotimes \nabla\Theta + \sin^2\Theta \nabla\Phi \bigotimes \nabla\Phi)$ is the damping dyadic, and W is the total vortex energy. The new terms due to spin transfer are $\vec{P}_\parallel = p_\parallel \int_{\mathrm{PC}} dV(\nabla\Theta \sin\Phi + \frac{1}{2}\nabla\Phi \sin 2\Theta \cos\Phi)$, which is the component of spin transfer parallel to the film plane, and $\vec{P}_\perp = p_\perp \int_{\mathrm{PC}} dV \sin^2\Theta \nabla\Phi$, which is the component of spin transfer perpendicular to the film plane. The unit vector $(\vec{p}_\parallel, p_\perp)$ represents the orientation of the incoming spin polarization and the subscript PC denotes an integral over the region underneath the point contact.

In the absence of pinning centers and by assuming that the sample edges are sufficiently far from the vortex core, the only position-dependent component of the vortex energy arises from the Oersted field generated from the current flow through the point contact. By assuming that the current flows through a perfectly cylindrical cross section in the free layer and that the vortex and Oersted field have the same polarity, we obtain for W in polar coordinates $W = -\mu_0 M_s H_I \int dV f(\vec{r}) \sin\Theta(\sin\varphi \cos\Phi - \cos\varphi \sin\Phi)$, where $f(\vec{r})$ describes the radial variation of the Oersted field amplitude H_I from the contact center. While it is difficult to evaluate this energy exactly, we find

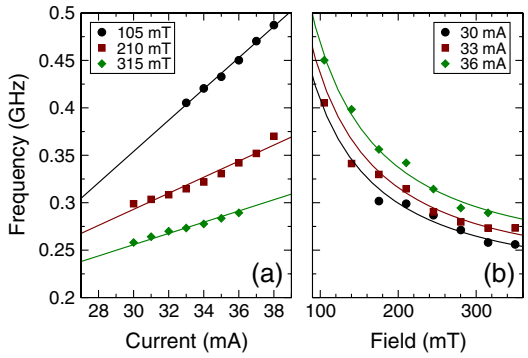

FIG. 3 (color online). Vortex oscillation frequency as a function of (a) applied current and (b) applied field. Dots are experimental data, and solid lines are fits based on Eq. (4).

numerically that the functional form $W(\rho) \simeq \kappa I \rho$ gives a reasonably good approximation for realistic Θ profiles.

The oscillation frequency is found by solving Eq. (1) in the rigid vortex approximation. By assuming that the vortex core is sufficiently far from the contact region, we suppose the gradient in the polar angle vanishes, $\nabla\Theta = 0$, and the polar angle is given by the uniform tilted angle due to the perpendicular applied field $\cos\Theta_0 = H/M_s$ within the contact region. By evaluating (1) within this approximation and using $R_0 \exp(i\psi) = X_0 + iY_0$, we find

$$\dot{R}_0 + \frac{\alpha D}{G} R_0 \dot{\psi} = \frac{\pi a^2 d}{G R_0} \sigma I p_\perp \sin^2\Theta_0, \tag{2}$$

$$\dot{\psi} - \frac{\alpha D}{G} \frac{1}{R_0} \dot{R}_0 = \frac{\gamma}{G M_s} \frac{1}{R_0} \frac{\partial W}{\partial R_0}, \tag{3}$$

where G and D are associated with the gyrovector and damping dyadic, respectively, a is the point-contact radius, and d is the film thickness. By assuming steady state oscillation for which $\dot{R}_0 = 0$ and $\omega \equiv \dot{\psi}$ is constant, we find a vortex precession frequency of

$$\omega = \left(\frac{1}{\pi a^2 d} \frac{\alpha D \kappa^2}{\sigma p_\perp}\right)\left(\frac{\gamma}{G M_s}\right)^2 \frac{I}{\sin^2\Theta_0}. \tag{4}$$

The field dependence is introduced through $\theta_0 = \cos^{-1}(H/M_s)$ and by approximating $p_\perp$ using the z component of the pinned-layer magnetization $p_\perp \simeq H/M_2$, where M_2 is the saturation magnetization of the pinned layer. Note that only the perpendicular component of the spin polarization leads to vortex precession; the in-plane component leads only to vortex core displacement. Here a nonvanishing $p_\perp$ arises from the finite tilt angle of the fixed layer magnetization by virtue of the perpendicular applied field.

A comparison between theory and experiment is shown in Fig. 3. We observe a quasilinear variation of the oscillation frequency with current in experiment, which is consistent with theory and is due to the linear dependence of the Oersted field energy on current. To produce the theoretical curves in Fig. 3(a), we first fit the $H = 105$ mT series using Eq. (4) and then use the theoretical H dependence to compute the slopes for the other applied fields, which are in good quantitative agreement with the experimental data. The theory also accounts for the frequency variation with applied field, as shown in Fig. 3(b). As before, we fit (4) to one data set ($I = 36$ mA) and used the predicted current variation for the other sets.

In summary, we have shown with experiment, simulation, and analytical theory that current-driven subgigahertz oscillations in point contacts are a result of large-amplitude vortex dynamics. The vortex attains a stable circular orbit outside of the contact region, whose frequency is governed by the applied perpendicular field and current.

This work was supported by the European Communities programs IST STREP, under Contract No. IST-016939 TUNAMOS, and "Structuring the ERA," under Contract No. MRTN-CT-2006-035327 SPINSWITCH, and by the Région Ile-de-France in the framework of C'Nano IdF. Q. M. acknowledges support from a CNRS/STMicroelectronics Ph.D. grant.

*joo-von.kim@u-psud.fr

[1] K. Y. Guslienko *et al.*, J. Appl. Phys. **91**, 8037 (2002).
[2] B. A. Ivanov and C. E. Zaspel, J. Appl. Phys. **95**, 7444 (2004).
[3] V. Novosad *et al.*, Phys. Rev. B **66**, 052407 (2002).
[4] J. P. Park *et al.*, Phys. Rev. B **67**, 020403(R) (2003).
[5] K. S. Buchanan *et al.*, Nature Phys. **1**, 172 (2005).
[6] V. Novosad *et al.*, Phys. Rev. B **72**, 024455 (2005).
[7] K. Y. Guslienko *et al.*, Phys. Rev. Lett. **96**, 067205 (2006).
[8] V. S. Pribiag *et al.*, Nature Phys. **3**, 498 (2007).
[9] J. Slonczewski, J. Magn. Magn. Mater. **159**, L1 (1996).
[10] L. Berger, Phys. Rev. B **54**, 9353 (1996).
[11] M. Tsoi *et al.*, Nature (London) **406**, 46 (2000).
[12] S. Kiselev *et al.*, Nature (London) **425**, 380 (2003).
[13] W. H. Rippard *et al.*, Phys. Rev. Lett. **92**, 027201 (2004).
[14] M. R. Pufall *et al.*, Phys. Rev. B **75**, 140404(R) (2007).
[15] J. Smit and H. G. Beljers, Philips Res. Rep. **10**, 113 (1955).
[16] A. N. Slavin and P. Kabos, IEEE Trans. Magn. **41**, 1264 (2005).
[17] O. Ertl *et al.*, J. Appl. Phys. **99**, 08S303 (2006).
[18] J. Xiao, A. Zangwill, and M. D. Stiles, Phys. Rev. B **70**, 172405 (2004).
[19] A. A. Thiele, Phys. Rev. Lett. **30**, 230 (1973).